How to cite: *Angew. Chem. Int. Ed.* **2024**, *63*, e202315064
doi.org/10.1002/anie.202315064

Photochemistry

Intramolecular Triplet Diffusion Facilitates Triplet Dissociation in a Pentacene Hexamer

Phillip M. Greißel[+], Dominik Thiel[+], Henrik Gotfredsen[+], Lan Chen, Marcel Krug, Ilias Papadopoulos, Mark Miskolzie, Tomás Torres, Timothy Clark, Mogens Brøndsted Nielsen, Rik R. Tykwinski, and Dirk M. Guldi**

Abstract: Triplet dynamics in singlet fission depend strongly on the strength of the electronic coupling. Covalent systems in solution offer precise control over such couplings. Nonetheless, efficient free triplet generation remains elusive in most systems, as the intermediate triplet pair $^1(T_1T_1)$ is prone to triplet-triplet annihilation due to its spatial confinement. In the solid state, entropically driven triplet diffusion assists in the spatial separation of triplets, resulting in higher yields of free triplets. Control over electronic coupling in the solid state is, however, challenging given its sensitivity to molecular packing. We have thus developed a hexameric system (HexPnc) to enable solid-state-like triplet diffusion at the molecular scale. This system is realized by covalently tethering three pentacene dimers to a central subphthalocyanine scaffold. Transient absorption spectroscopy, complemented by theoretical structural optimizations and steady-state spectroscopy, reveals that triplet diffusion is indeed facilitated due to intramolecular cluster formation. The yield of free triplets in HexPnc is increased by a factor of up to 14 compared to the corresponding dimeric reference (DiPnc). Thus, HexPnc establishes crucial design aspects for achieving efficient triplet dissociation in strongly coupled systems by providing avenues for diffusive separation of $^1(T_1T_1)$, while, concomitantly, retaining strong interchromophore coupling which preserves rapid formation of $^1(T_1T_1)$.

Introduction

Solar energy conversion invariably suffers from intrinsic loss processes. In conventional single-junction photovoltaic cells, these losses restrict the overall efficiency to an upper thermodynamic limit. The latter is approximately 33%, which is also referred to as the detailed-balance limit.[1–5] Minimizing such loss processes and boosting the efficiency of solar cells is highly desired and has initiated significant efforts. In particular, thermalization, i.e., the loss of the excess energy as heat from photons above the band gap of the material, is a major loss channel. One way to reduce energy loss is through the down-conversion of high-energy photons; in other words, by converting excited states with energies exceeding twice that of the band gap energy into two charge carriers. In quantum dots or semiconductor nanocrystals, this phenomenon is called multiple exciton generation (MEG).[1,4,6–8] At the molecular scale, the corre-

[*] P. M. Greißel,[+] D. Thiel,[+] M. Krug, I. Papadopoulos, D. M. Guldi
Department of Chemistry and Pharmacy & Interdisciplinary Center for Molecular Materials (ICMM), Friedrich-Alexander-University Erlangen-Nuremberg
Egerlandstraße 3, 91058 Erlangen (Germany)
E-mail: dirk.guldi@fau.de

H. Gotfredsen,[+] L. Chen, M. Miskolzie, R. R. Tykwinski
Department of Chemistry, University of Alberta
11227 Saskatchewan Drive, Edmonton, Alberta, T6G 2G2 (Canada)
E-mail: rik.tykwinski@ualberta.ca

H. Gotfredsen,[+] M. Brøndsted Nielsen
Department of Chemistry, University of Copenhagen
Universitetsparken 5, 2100 Copenhagen Ø (Denmark)

H. Gotfredsen[+]
Current address: Department of Chemistry, University of Oxford, Chemistry Research Laboratory
Oxford OX1 3TA (UK)

I. Papadopoulos
Department of Applied Chemistry, Graduate School of Engineering, Center for Molecular Systems (CMS), Kyushu University
744 Motooka, Nishi-ku, Fukuoka 819-0395 (Japan)

T. Torres
Department of Organic Chemistry and Institute for Advanced Research in Chemical Sciences (IAdChem), Universidad Autónoma de Madrid
Campus de Cantoblanco, 28049 Madrid (Spain)

T. Torres
IMDEA Nanociencia
C/Faraday 9, Cantoblanco, 28049 Madrid (Spain)

T. Clark
Department of Chemistry and Pharmacy & Computer-Chemie-Center (CCC), Friedrich-Alexander-University Erlangen-Nuremberg
Nägelsbachstraße 25, 91052 Erlangen (Germany)

[+] These authors contributed equally to this work.

sponding analogue of MEG is known as singlet fission (SF).[6,9,10]

The overall process of SF involves the conversion of one singlet excited state (S_1) of one chromophore into two independent triplet excited states (T_1+T_1) spanning two chromophores.[6,7] In principle, SF allows a doubling of the photocurrent generation.[11–14] Hence, SF offers great potential for harnessing solar energy, as implementing SF materials in photovoltaics could circumvent the current threshold of conventional silicon-based solar cells. As a matter of fact, SF could increase the power conversion efficiency limit to approximately 45 %.[15–18] SF is best described by the simplified kinetic model shown in equation 1, which includes two intermediate triplet pair states in order to adequately model the triplet dissociation process.[11,14,19–21]

$$S_1S_0 \rightleftharpoons {}^1(T_1T_1) \rightleftharpoons {}^M(T_1\cdots T_1) \rightleftharpoons (T_1 + T_1) \quad (1)$$

The correlated triplet pair state, $^1(T_1T_1)$, is formed initially with both triplet excited states being strongly coupled. Spin multiplicity is maintained for $^1(T_1T_1)$, whereas the subsequent state $^M(T_1\cdots T_1)$ is not spin-pure anymore and corresponds to a pair of weakly interacting triplets that have lost their electronic and vibrational coupling, while remaining spin-entangled. Finally, $^M(T_1\cdots T_1)$ decays into the uncorrelated triplet pair (T_1+T_1) via spin-dephasing, resulting in two non-interacting triplet excited states.[11,14]

Fundamental criteria for SF include, first, the energy matching condition $E(S_1) \sim 2E(T_1)$, as well as $E(T_2) > 2E(T_1)$.[7] The former renders SF exergonic, while the latter precludes the population of higher-lying triplet excited states. To this end, pentacene is an ideal model system.[6,7,22] Second, excited-state interaction(s) between chromophores (i.e., coupling) is required. The extent of coupling between the chromophores affects SF dynamics and is governed by the structure, spatial separation, and orientation of the chromophores.[23–25] In the solid state, interchromophoric coupling is dictated by crystal packing, whereas in solution, the coupling can be controlled in covalent structures through the topology and electronic nature of the linker connecting the chromophores.[26–32]

If the fundamental SF criteria are met, a correlated triplet pair state $^1(T_1T_1)$ of overall singlet character is formed following photoexcitation to (S_1S_0). At this stage, the two triplet excited states are situated on two neighboring chromophores. Since spin multiplicity is maintained, the first step is spin-allowed and, consequently, can occur on ultrafast timescales (ca. femto- to picoseconds) with efficiencies approaching unity.[33,34] The formation of $^1(T_1T_1)$ is also referred to as the internal conversion step of SF.[6] Various mechanisms have been proposed for the formation of $^1(T_1T_1)$. On one hand, SF can proceed via an incoherent process in a direct or indirect manner.[6,35,36] The latter involves an intermediate state with partial charge-transfer character, which may be real or virtual, depending on the relative energies of the involved states.[30,37–40] On the other hand, SF can proceed coherently via a vibronic coupling mechanism involving the superposition of the first singlet excited state, the correlated triplet pair state, and potentially a charge-transfer state.[9,11,22,23,30,37,41–46]

Strong interchromophoric coupling favors SF by accelerating the internal conversion rate of $^1(T_1T_1)$, such that it outcompetes alternative radiative and non-radiative relaxation channels. This design criterion comes, however, at a cost. Strong electronic coupling also promotes geminate triplet-triplet annihilation (TTA),[33,47–50] preventing the dissociation of $^1(T_1T_1)$ into the uncorrelated triplet pair (T_1+T_1) in the second step of SF. Hence, when considering SF in its entirety, electronic coupling alone is inadequate to achieve an optimal balance between the first and second steps of SF and the associated deactivation channels.[49]

Practical applications based on SF remain challenging due to several unresolved drawbacks.[51] For instance, materials that rely on intramolecular SF (*i*-SF) are easily integrated into devices, but they are plagued by efficient TTA. As such, they fail to produce long-lived triplet excited states,[52–54] which impairs efficient charge carrier injection into semiconductors.[17,55] Reducing losses due to TTA can be accomplished by moderating the electronic coupling in order to increase triplet excited-state lifetimes. Among other strategies, electronic coupling can be weakened by either structural reorganization, such as torsional and rotational molecular motion, or vibronic coupling to neighboring molecules, which is essentially a diffusive spatial separation of the triplets in extended systems.[14,44,52,56,57] In both scenarios, the exchange couplings between the triplets of the correlated triplet pair $^1(T_1T_1)$ are modulated with respect to their relative orientation and separation distance.[48,58–60] For weaker intertriplet coupling, the energy gap between the singlet $^1(T_1T_1)$ and quintet correlated triplet pair state $^5(T_1T_1)$ is reduced exponentially (particularly in case of greater separation distances between the two triplets of the pair due to diffusion) and allows for singlet-quintet mixing.[58,59,61,62] Hence, a spatial separation of $^1(T_1T_1)$ via triplet diffusion may prove to be the most effective way to enhance dissociation, because triplet excited states can easily hop in larger arrays with three or more repeating units. Following diffusion, the greater distances between the two triplet excited states effectively lower the triplet-triplet exchange coupling and, thus, sufficiently reduce the triplet-triplet binding energies.[58,60,63–65] The gain in entropy constitutes the driving force for overcoming the $^1(T_1T_1)$ binding energy in extended systems.[59,66] In molecular dimers, however, triplets of $^1(T_1T_1)$ are spatially confined, and efficient triplet dissociation requires significant mixing of $^1(T_1T_1)$ and $^5(T_1T_1)$. In strongly coupled dimers, $^5(T_1T_1)$ is too high in energy and spin mixing with $^1(T_1T_1)$ becomes impossible, which ultimately results in efficient TTA.[48] Significant spin mixing of $^1(T_1T_1)$ and $^5(T_1T_1)$ is only possible for covalent dimers exhibiting weak interchromophore coupling, due to a reduced energy gap between $^1(T_1T_1)$ and $^5(T_1T_1)$. While spin mixing of $^1(T_1T_1)$ and $^5(T_1T_1)$ boosts the yield of free triplet excited states,[57] it comes at the expense of slower $^1(T_1T_1)$ formation (i.e., slower SF), due to the weaker interchromophore coupling.[9,11,14,20,44,52,58,67–70]

In general, delocalization plays a major role in the dynamics of SF, as it is not only relevant for the triplet

dissociation, but also for the initial event of SF.[71] As triplet excited states are more localized compared to singlet excited states (which translates to an increased number of available microstates for $^1(T_1T_1)$ compared to (S_1S_0)), the first event of SF also entails a gain in entropy in extended systems.[51,63] Such effects are, however, predominantly observed in solid-state systems, and they are less significant in solution where excited states are confined within the molecular structure.[9,11,14,72]

To date, the majority of studies have focused on the first step of *i*-SF, that is, formation of $^1(T_1T_1)$, and these efforts have greatly benefitted our understanding of the requirements for rapid and efficient generation of $^1(T_1T_1)$. The spatially separated triplet pair and its significance in the dissociation process, however, still remains largely unexplored due, in part, to its absence in most covalent systems. The lack of distinct optical spectroscopic features poses another significant challenge, especially for discriminating between $^1(T_1T_1)$, $^M(T_1\cdots T_1)$, and (T_1+T_1).[52] Recently, oligomeric systems have been probed to elucidate the process(es) of triplet dissociation. At the focal point have been either (a) linear chain-like structures,[9,10,51,52,63,73] or (b) dendrimeric structures that exhibit some through-space orbital interactions to mimic geometries and interactions within solids.[54,74–76]

In this work, we present a molecular system for overcoming the challenging task of unifying fast formation of the correlated triplet pair, $^1(T_1T_1)$, with its efficient decorrelation into free triplets, i.e., T_1+T_1. Inspired by the efficient evolution of $^1(T_1T_1)$ into free triplets in solid-state pentacene by triplet diffusion, we rationalized that a suitable molecular system could be realized by drawing upon design principles from both solution and the solid state. Consequently, we devised HexPnc as a molecular system to mimic solid-state triplet hopping (Figure 1). The dendrimeric structure, HexPnc, combines three pentacene dimers joined to a central C_3-symmetrical subphthalocyanine (SubPc) core. Each pentacene dimer contains a *meta*-phenylene spacer to ensure a favorable arrangement of pentacenes to achieve fast *i*-SF with an efficient formation of $^1(T_1T_1)$.[29] The unique symmetry and curvature features of SubPc makes it an appropriate scaffold from which to branch off *i*-SF units, i.e., the pentacene dimers, while still ensuring a close spatial separation between each of them, needed for triplet diffusion.[77] The spatial arrangement in HexPnc is designed to allow for diffusive separation of the correlated triplet pair state and, hence, facilitates free triplet formation via decoherence/dephasing. To understand the photophysics of HexPnc, we contrast its behavior to that of DiPnc. The latter is restricted to a single *meta*-phenylene pentacene dimer joined to a SubPc in an equatorial position and, thus, cannot facilitate spatial separation of $^1(T_1T_1)$ as both triplets of the pair are confined to the dimer. The propensity of SubPc to function as an efficient light harvesting antenna and sensitizer for *i*-SF in DiPnc via intramolecular Förster resonance energy transfer (*i*-FRET) has been documented.[78] Although it is not the focus of this work, all evidence points to SubPc operating in a similar manner in HexPnc, thereby enhancing the *i*-SF response through

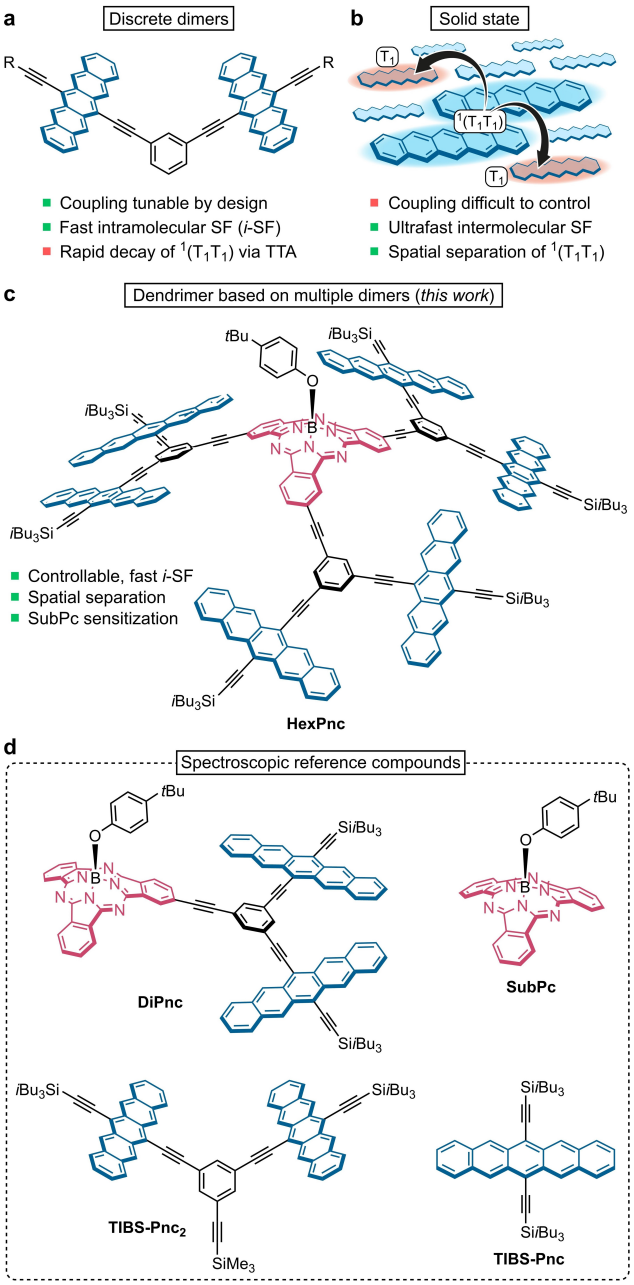

Figure 1. Conceptual design of HexPnc unites the advantageous attributes of a discrete dimer with those of solid-state pentacene. (a) Fast (picosecond timescale), controllable intramolecular singlet fission (*i*-SF) occurs in dimers often accompanied by concurrent, fast deactivation of the correlated triplet pair state $^1(T_1T_1)$ through triplet-triplet annihilation (TTA). R = solubilizing group. (b) Through spatial separation via triplet diffusion, ultrafast (subpicosecond timescale) SF in the solid state forms free triplets, although the process is challenging to control because interchromophore coupling is dictated by molecular packing. (c) The structure of HexPnc investigated in this work. (d) Structures of spectroscopic reference compounds (TIBS = tri-*iso*-butylsilyl).

SubPc absorption and subsequent energy transfer to the pentacene dimers. In that sense, HexPnc unites several attributes, which are attractive in solar energy conversion devices, that is, efficient light harvesting, fast and efficient *i*-

SF, and enhanced decoherence of the SF intermediate $^1(T_1T_1)$.

We employ ultrafast transient absorption spectroscopy, kinetic modeling, and quantum chemical calculations to elucidate triplet generation and deactivation in HexPnc. Quantum chemical calculations support the photophysical involvement of an unsymmetrical conformer of HexPnc, in which two pentacene dimer moieties interact to form an intramolecular cluster, while the third pentacene dimer remains isolated. HexPnc thus constitutes a synthetic model system for establishing the influence of triplet diffusion on *i*-SF performance in extended systems, in general, and on the fate of the $^1(T_1T_1)$, in particular. These findings correlate our understanding of *i*-SF triplet dynamics with the ultimate goal of facilitating triplet diffusion in condensed state (e.g., solids, films, etc.), which is a requisite for implementation of *i*-SF materials in practical applications.[3,79]

Results and Discussion

Synthesis and Characterization

HexPnc was synthesized by means of a three-fold Sonogashira reaction between the C_3-symmetrical triiodo-SubPc building block **1**[80–82] and pentacene dimer **2** (Scheme 1).[78] An apical *tert*-butylphenoxy ligand bound to the boron atom was used to provide solubility. Using size-exclusion chromatography, HexPnc was isolated as the eluting species of highest molecular weight. The identity of HexPnc has been confirmed by MALDI mass spectrometry (*m/z* found, 3977.9546; calc. for $C_{286}H_{265}{}^{11}BN_6OSi_6$ (M^+), 3977.9573) as well as ^1H, ^{13}C, and ^{11}B NMR spectroscopy (see SI, Section 4).

Ground- and excited-state interactions in the conjugates

Steady-state absorption experiments in both toluene and benzonitrile have been performed (Figures 2a and S14; Table S1). In both solvents, the absorption spectrum of DiPnc is approximately a linear superimposition of the individual components (Figures S15a and S16a). Most notably, the spectrum of DiPnc comprises a strong, distinct

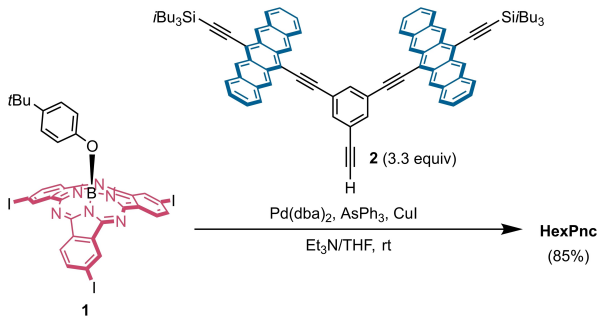

Scheme 1. Synthesis of HexPnc with a central SubPc and three peripheral pentacene dimers.

absorption at around 580 nm corresponding to the Q-band absorption of SubPc, combined with the well-resolved vibronic fine structure of TIBS-Pnc_2 in the range from 550 to 660 nm. Only the SubPc Q-band absorption is affected by the peripheral substitution of the SubPc, that is, a small redshift and a slight change in shape. The lack of significant changes in the spectrum of DiPnc confirms that only minor electronic interactions are present in the ground state, as previously documented.[78] The absorption features of HexPnc, in both toluene and benzonitrile, contrast those of DiPnc and do not reflect the vibronic progression of absorptions characteristic of pentacene derivatives in solution, which employ acetylene-π-linker-acetylene moieties.[29,78] Instead, the absorption spectrum of HexPnc strongly reflects the features of a drop-cast film of 6-13-bis(triisobutylsilylethynyl)pentacene (TIBS-Pnc).[72] In comparison to TIBS-Pnc_2, the vibrational fine structure of HexPnc is poorly resolved, exhibits a greater oscillator strength of the pentacene centered 0–1* transition with respect to the 0–0* band (characteristic for H-type aggregation), and appears broadened (Figure 2a).[83,84] Similar observations have been made for strongly coupled pentacene dimers, which exhibit substantial through-space interactions, such as an *ortho*-phenylene-linked pentacene dimer investigated by Zirzlmeier et al.,[29] or the xanthene-bridged pentacene dimers studied by Basel et al.[85] In sound agreement, the molar extinction coefficient (ε) of the pentacene 0–0* transition for HexPnc is significantly lower than that expected for three isolated pentacene dimers (Figures S15b and S16b; Table S1). Lastly, contributions from the SubPc moiety are hardly discernable. Overall, we infer strong ground-state interactions and deduce that they stem from intramolecular pentacene stacking, given the concentration independence of these features (Figure S17).[86] This is consistent with computational modeling of the DiPnc and HexPnc structures.[87] Conformational analysis and subsequent geometry optimization predicts unsymmetrical structures for HexPnc as the energetic minimum in which two of the pendent pentacene dimers associate to form an intramolecular cluster (Pnc_4), resembling packing in the solid state, while the third dimer moiety (Pnc_2) remains isolated (Figure 2b).[88] Within Pnc_4, two pentacenes from two different dimers are oriented in a slightly twisted slip-stacked arrangement. The minimal pentacene center-to-center distance is roughly 4.8 Å, which deviates significantly from that in both DiPnc and the Pnc_2 subunit of HexPnc, both of ca. 11.4 Å (Figures S50 and S51; Table S7). The intimate pentacene-pentacene arrangement is the origin of strong through-space couplings, as indicated by the lifted degeneracy of the frontier orbitals for HexPnc (Figures S40 and S41), and is responsible for the increased oscillator strength of the pentacene centered 0–1* transition within Pnc_4 compared to Pnc_2 as well as DiPnc.[72,89]

Steady-state fluorescence spectroscopy was carried out to screen for potential excited-state interactions. With the known *i*-FRET from SubPc to Pnc_2,[78] the fluorescence spectra were recorded upon photoexcitation at 500 nm into the Q-band absorption of SubPc. For DiPnc, weak emission centered at ca. 590 and 670 nm is discernible in both toluene

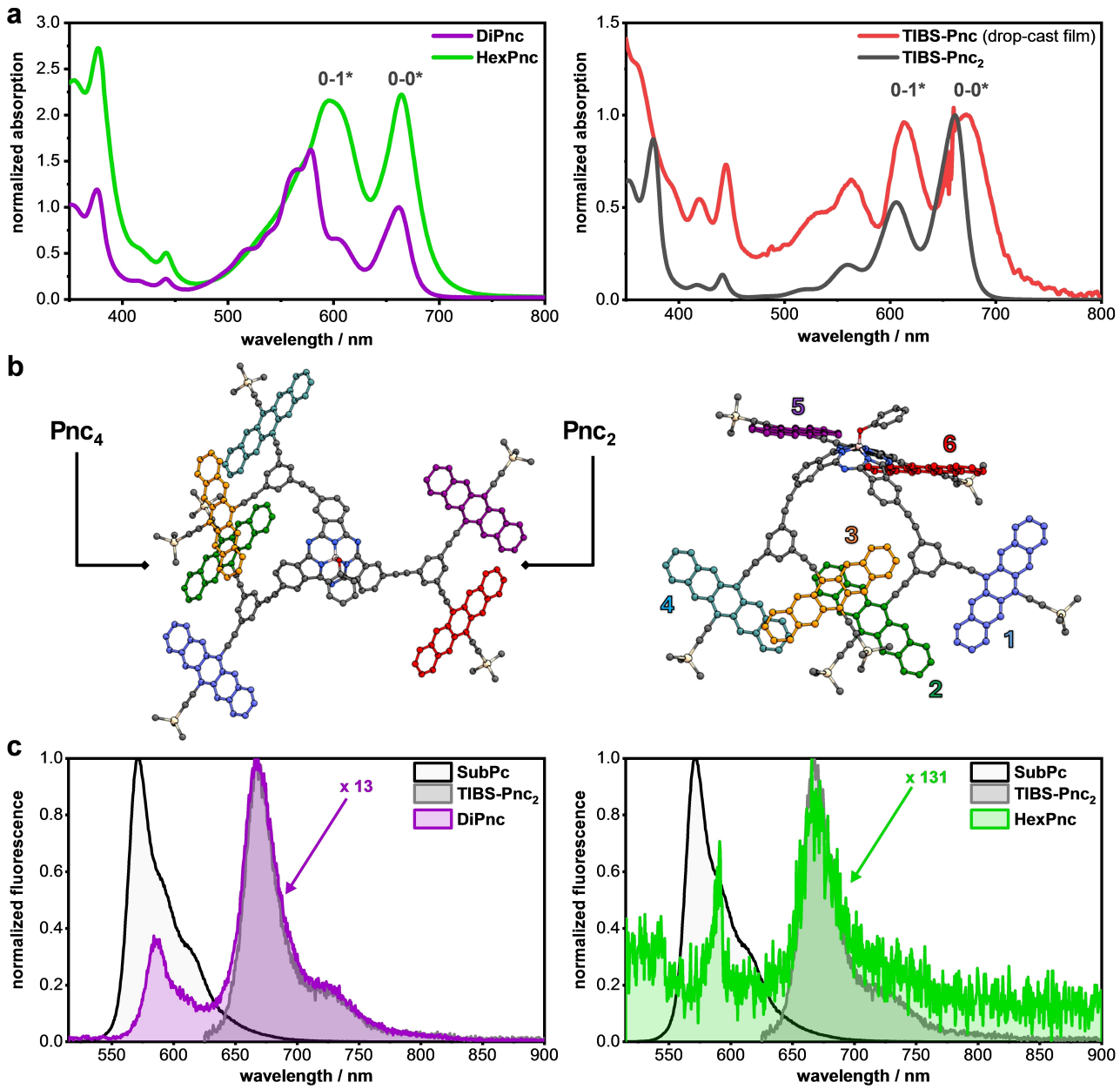

Figure 2. (a) Steady-state absorption spectra of DiPnc (purple) and HexPnc (green) recorded in toluene at room temperature (both spectra were normalized with respect to the longest-wavelength absorption maximum of DiPnc) in comparison to the normalized steady-state absorption spectra of a drop-casted film of TIBS-Pnc (red) as well as TIBS-Pnc_2 (grey), recorded in toluene at room temperature. Spectra were normalized with respect to the corresponding longest-wavelength absorption maximum. (b) Geometry-optimized structure of HexPnc obtained at the B3LYP +GD3BJ/def2SVP level using a C_3-symmetrical structure (+25.3 kcal/mol[90,91]) as starting geometry (see SI, Section 8 for computational details). The structure is displayed from different viewing angles for better visualization of the intramolecular cluster (Pnc_4). The various pentacene chromophores are numbered as used in the following section. (c) Normalized steady-state fluorescence spectra of DiPnc (left) and HexPnc (right) including their corresponding individual building blocks in toluene at room temperature. Spectra of the target materials as well as of the reference SubPc were recorded upon photoexcitation at 500 nm, whereas spectra of TIBS-Pnc_2 were recorded upon photoexcitation at 610 nm. Optical densities were roughly 0.0250 at the excitation wavelength for all samples. All spectra were normalized with respect to the fluorescence maximum of SubPc.

and benzonitrile (Figures 2c and S18a; Table S2). The former stems from the SubPc, while the latter originates from the pentacene moieties. Both fluorescence bands are, however, almost quantitatively quenched in comparison to the corresponding reference compounds SubPc and TIBS-Pnc, exhibiting fluorescence quantum yields (FQYs) of 0.3 % and 1.1 %, respectively. The observed FQYs are consistent with the sequence of efficient *i*-FRET and *i*-SF, as described previously.[78,92,93] The fluorescence of HexPnc is further reduced (excitation at 500 nm), evidenced by a pentacene originated FQY of less than 0.1 % regardless of the solvent (Figures 2b and S18b; Table S2) and a com-

pletely quenched SubPc centered fluorescence. The drastically lowered fluorescence from HexPnc in the presence of three pentacene dimers as energy acceptors is consistent with efficient *i*-FRET followed by *i*-SF.

Triplet evolution dynamics

Femtosecond transient absorption (fsTA) experiments were first performed to provide insight into the pentacene-related dynamics, that is, the early steps of *i*-SF, including the dynamics of triplet evolution. To this end, an excitation wavelength of 660 nm was used to exclusively excite the pentacene moieties. At first glance, the dynamics of DiPnc and HexPnc are quite similar. Both show the immediate development of features distinctive of the first singlet excited state of pentacene (S_1) irrespective of the solvent (Figure 3).[29] These spectral characteristics include excited-state absorptions (ESAs) in the visible region at ca. 450 and 590 nm, as well as ground-state bleaching (GSB) in the range of 600–700 nm. As time progresses, the features of (S_1) gradually decay concomitantly with the rise of strong ESAs at ca. 470 and 510 nm and GSB in the range from 550–700 nm due to the formation of the first triplet excited state of pentacene. Triplet features are formed on the picosecond time scale at the expense of (S_1), consistent with *i*-SF.[29] Notably, *i*-SF can be induced not only via direct excitation of the pentacene units, but also via excitation of the SubPc core that, upon photoexcitation at 532 nm, serves as an energy donor and transfers the excitation energy to the pentacene units. The exact nature of this has been reported elsewhere and, therefore, is not discussed in detail here (Figures S19 and S20a–S22a).[78] Closer inspection of the triplet evolution at 510 nm for DiPnc and HexPnc, however, reveals subtle differences in the initial deactivation dynamics, namely the maximum triplet population is reached after approximately 80 ps in HexPnc compared to the ca. 260 ps for DiPnc in toluene (Figures 3 and S19–S22).

Since we hypothesize different contributions of Pnc_2 and Pnc_4 to the overall oscillator strengths in the 0–0* and 0–1*

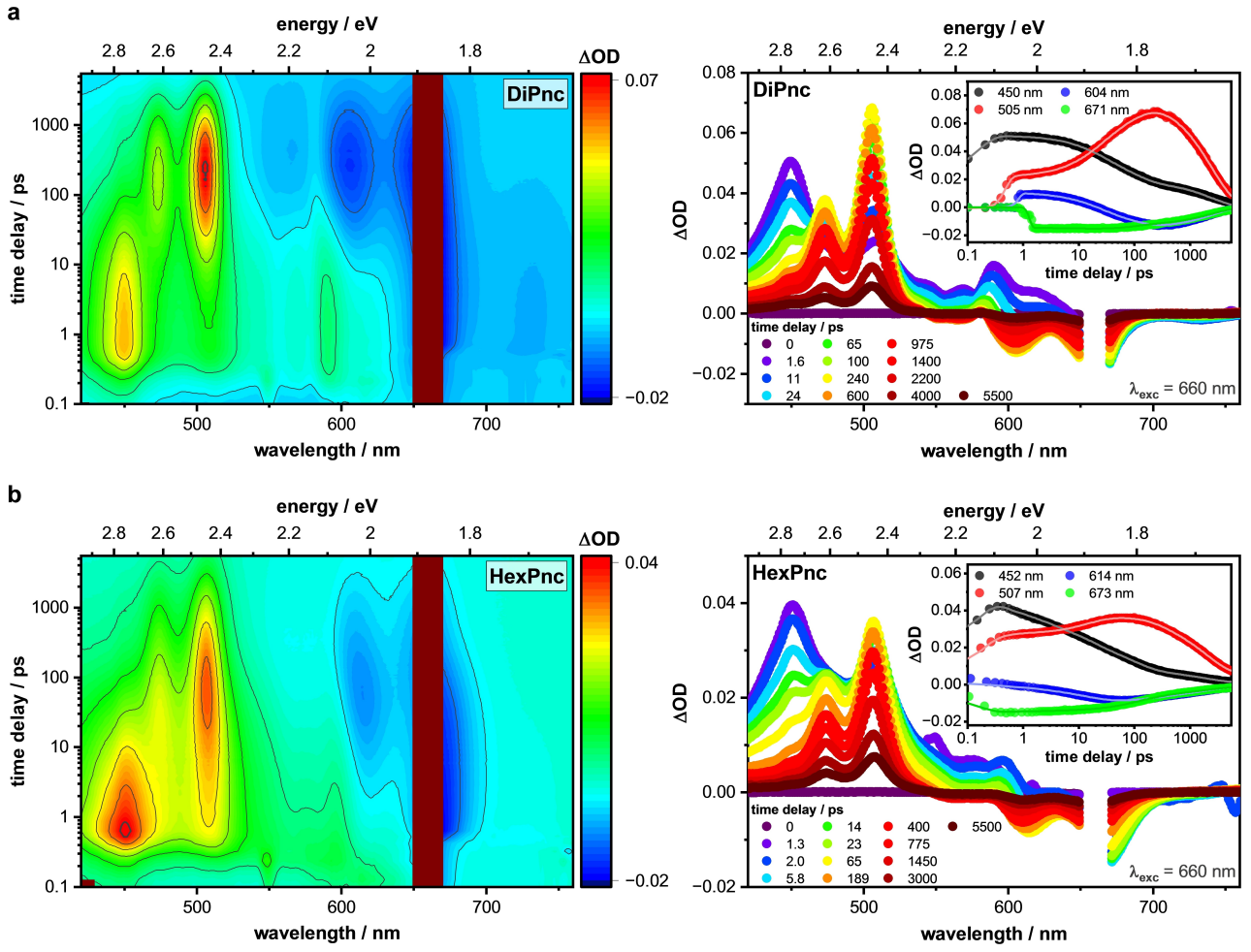

Figure 3. Chirp and zero-point corrected differential absorption spectra of (a) DiPnc and (b) HexPnc obtained from femtosecond transient absorption experiments upon photoexcitation at 660 nm (400 nJ) in argon-saturated toluene at room temperature with various time delays between 0 and 5500 ps. Left – 2D heat map of the recorded differential absorption spectra. Right – Differential absorption spectra at selected time delays. Time absorption profiles as well as corresponding fits of selected wavelengths are depicted in the inset (for exact values, see corresponding figure legend).

transitions of HexPnc (Figure 2a), we explored additional excitation wavelengths to assess the influence on the excited-state dynamics. Intriguingly, we observe an excitation wavelength dependency of the triplet evolution for HexPnc (Figure 4).[94] Triplet formation is accelerated when exciting into the higher energy edge of the pentacene absorption ($\lambda_{exc} \leq 633$ nm). Since SF is exergonic for pentacene derivatives, we rationalize that faster triplet evolution stems solely from a more pronounced excitation into the Pnc_4 subunit, due to the greater oscillator strength of the 0–1* transition compared to Pnc_2 (Figure 2a), and not from excitation of excess vibrational quanta.[95] Thus, modulation of the excitation wavelength allows for manipulation of the ratio of excitation into the Pnc_4 or Pnc_2 chromophore units of HexPnc. As reasoned from the optimized geometry of HexPnc and its orbital interaction diagram, the spatial orientation of pentacenes 2 and 3 (see Figure 2b for numbering of pentacene units) within Pnc_4 fosters exceptionally strong through-space interactions that render this site a coupling hotspot within Pnc_4 (Figures S40 and S41; Table S7). The result is the rapid first step of *i*-SF, namely $^1(T_1T_1)$ formation. Therefore, photoexcitation of Pnc_4, rather than Pnc_2, leads to an acceleration of the overall *i*-SF rates.[96]

It is worth mentioning that the triplet decay in HexPnc is slower than in DiPnc. Toward the end of the time delays of the fsTA setup (ca. 5500 ps), triplet features are still discernable for HexPnc despite reaching maximum population at considerably earlier time delays than for DiPnc. All observed trends remained unaffected when increasing the solvent polarity, i.e., moving from toluene to benzonitrile (Figure S23).

Triplet deactivation dynamics

The triplet excited-state deactivation is unresolvable on the femtosecond time scale, and we thus performed complementary transient absorption experiments on the nanosecond time scale (nsTA). In both toluene and benzonitrile, DiPnc shows the triplet excited state signatures of pentacenes, that is, ESAs at around 470 and 510 nm along with GSB in the range from 550 to 700 nm (Figures 5a, S24, and S26). These features evolve immediately after photoexcitation at 660 nm and then decay tri-exponentially. Based on previous reports, the first species is ascribed to the correlated triplet pair state $^1(T_1T_1)$ due to its fast formation.[29,68] The second species is the weakly coupled triplet pair state $^M(T_1\cdots T_1)$. This state is spin-entangled but has lost its electronic and vibronic coherence via torsional and rotational motions within the structure.[97,98] These structural changes modulate the triplet-triplet exchange couplings and, in turn, enable a mixing of $^1(T_1T_1)$ and $^5(T_1T_1)$.[51,56] The process likely occurs in low yields, especially in strongly coupled systems, as it is the case for phenylene-linked dimers.[66] The lifetime of the third component is on the order of microseconds and allows for the unambiguous assignment of the free triplet excited states (T_1+T_1). Increasing the solvent polarity affects neither the triplet decay dynamics nor the yields of free triplets of DiPnc (Figures 5a and S26b). The triplet deactivation dynamics of HexPnc vary significantly from those of DiPnc. Most notably, a considerably higher population of free triplets is observable, independent of the solvent polarity (Figures 5b, S25, and S27). A more in-depth analysis of the deactivation dynamics, in general, and the triplet decay kinetics, in particular, is given in the next section.

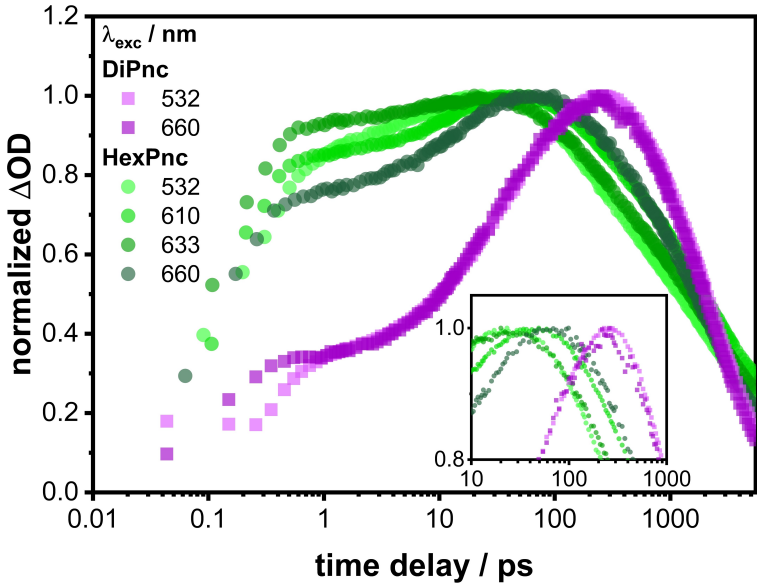

Figure 4. Triplet evolution dynamics – single-wavelength kinetics at the respective excited state absorption maximum of the pentacene related first triplet excited state (≈510 nm) of DiPnc (purple) and HexPnc (green) recorded for different excitation wavelengths (see figure legend for exact values) in femtosecond transient absorption experiments in argon-saturated toluene at room temperature within time delays ranging from 0 to 5500 ps. The inset shows the kinetic traces within a narrower time interval for better visibility.

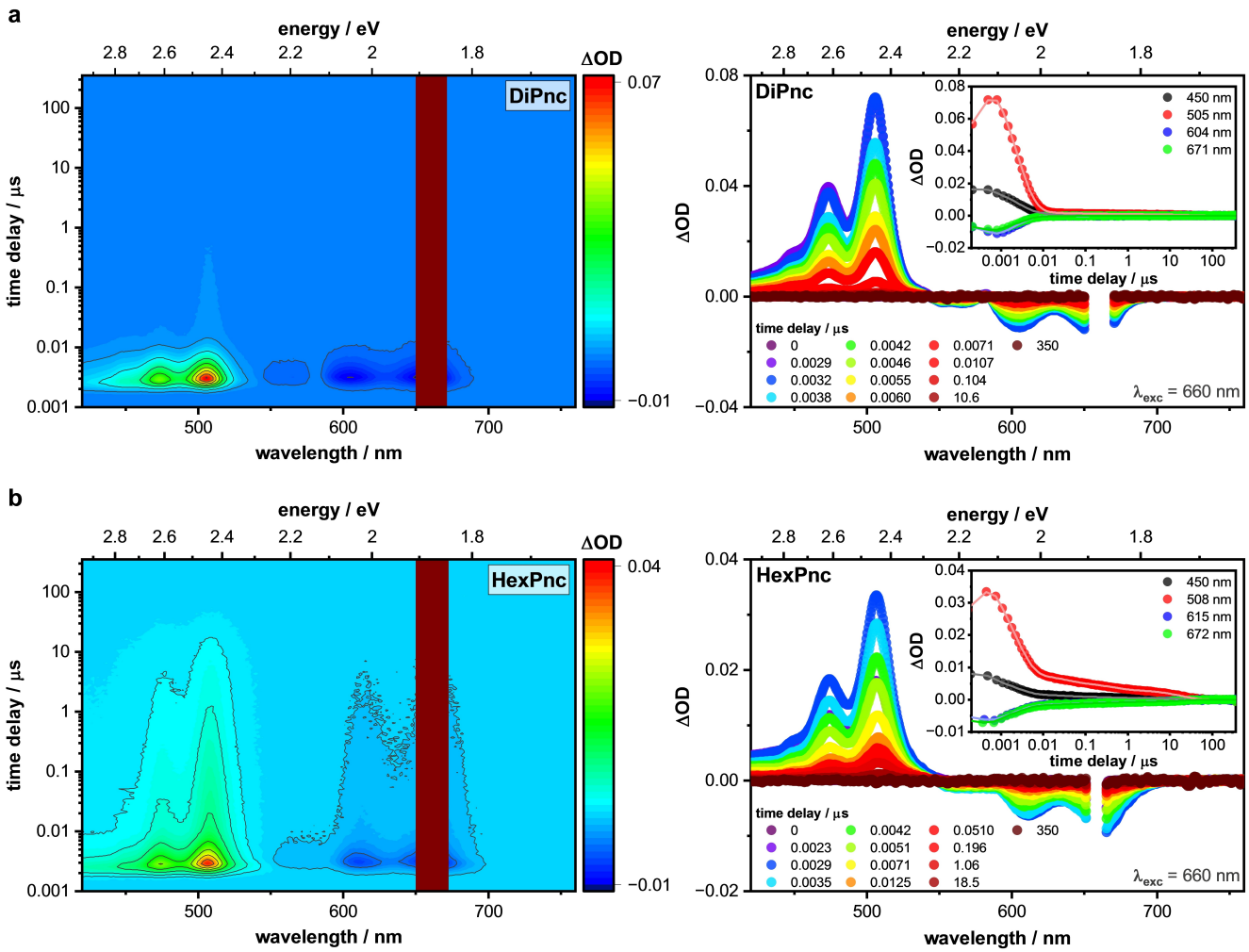

Figure 5. Zero-point corrected differential absorption spectra of (a) DiPnc and (b) HexPnc obtained from nanosecond transient absorption experiments upon photoexcitation at 660 nm (400 nJ) in argon-saturated toluene at room temperature with various time delays between 0 and 360 µs. Left – 2D heat map of the recorded differential absorption spectra. Right – Differential absorption spectra at selected time delays. Time absorption profiles as well as corresponding fits of selected wavelengths are depicted in the inset (for exact values, see corresponding figure legend).

A closer look at the triplet decay reveals an increase in triplet population at shorter excitation wavelengths ($\lambda_{exc} \leq$ 633 nm) for HexPnc, whereas the populations remain unchanged for DiPnc (Figures 6 and S28). In line with faster *i*-SF rates at higher pump energies for HexPnc, we attribute greater population of the free triplets to a higher fraction of photoexcitation of Pnc_4. The presence of multiple pentacenes in close proximity within the Pnc_4 subunit provides sufficient statistical space for the triplets of the triplet pair, initially formed at the coupling hotspot (pentacenes 2 and 3), to hop to adjacent pentacenes via Dexter triplet-triplet energy transfer.[21,60,99] Entropically driven spatial separation of the triplet pairs facilitates the loss of electronic and vibronic coherence and, eventually, after subsequent spin dephasing, culminates in the observed higher yields of (T_1 + T_1) (exact yields are given in the following kinetic modeling section). In stark contrast, upon excitation favoring Pnc_2 (λ_{exc} = 660 nm), the initial correlated triplet pair is spatially confined. Triplets cannot diffuse apart and, therefore, remain strongly coupled. They are prone to undergo fast intramolecular TTA, resulting in the recovery of the electronic ground state, while dissociation into free triplets is suppressed.[100] In short, the excited-state deactivation in HexPnc can be directed toward either of two distinct channels through selection of an excitation wavelength that targets either Pnc_4 or the Pnc_2. Because the two channels involve different overall rates of *i*-SF and yields of free triplets generated, this constitutes a way of tuning the SF dynamics of HexPnc. On the contrary, DiPnc lacks such a dependency on the excitation wavelength.

Kinetic modeling

The presence of two parallel deactivation channels for HexPnc was supported by several factors, including 1) the spectral resemblance of HexPnc to that of pentacene thin-films, 2) the wavelength dependence of both the rates of *i*-

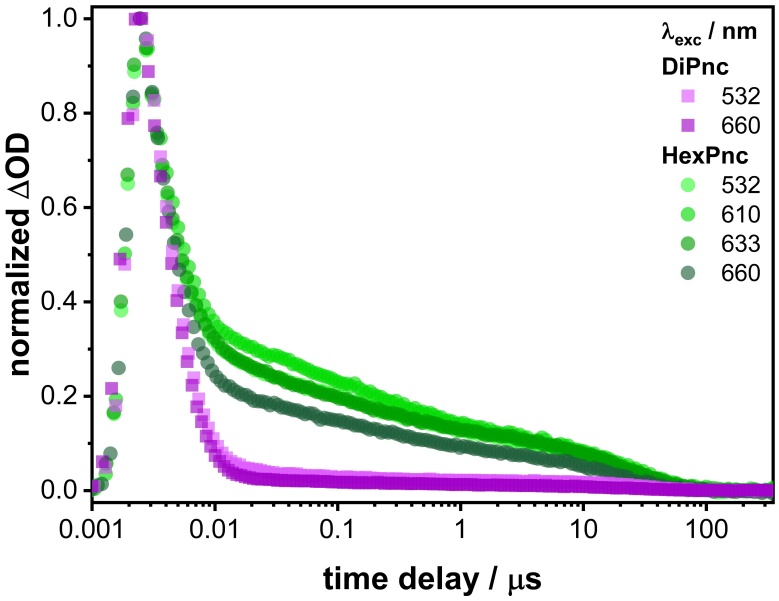

Figure 6. Triplet decay dynamics – single wavelength kinetics at the respective excited state absorption maximum of the pentacene related first triplet excited state (≈510 nm) of DiPnc (purple) and HexPnc (green) recorded for different excitation wavelengths (see figure legend for exact values) in nanosecond transient absorption experiments in argon-saturated toluene at room temperature within time delays ranging from 0 to 360 μs.

SF and yields of free triplets, and 3) the unusual triplet deactivation dynamics corroborated by geometry optimizations. Thus, we sought a kinetic model to fit the observed deactivation dynamics of HexPnc and, in particular, to differentiate between unique channels originating from excitations of Pnc_2 and Pnc_4.[101] The excitation ratio between the Pnc_2 and Pnc_4 channels is influenced primarily by the excitation wavelength, which assists in deconvolution of the dynamics (Figure 7). A description of the individual models, and their limitations, to fit the fsTA and nsTA data is given in the Supporting Information (Figures S29 and S34).

For DiPnc, $(S_1)_{Pnc2}$ decays to an intermediate state with partial charge-transfer character $(M)_{Pnc2}$ on its way to $^1(T_1T_1)_{Pnc2}$, as shown in previous work on analogous SubPc-Pnc_2 conjugates (Figures S30 and S32).[78] Subsequently, $^1(T_1T_1)_{Pnc2}$ either loses its electronic and vibronic coherence and forms $^M(T_1\cdots T_1)_{Pnc2}$, or deactivates back to the electronic ground state via TTA. Torsional and rotational motion are the only feasible options for loss of electronic and vibronic coherence in $^1(T_1T_1)_{Pnc2}$, as spatial separation of two triplet excited states is impossible due to confinement within the pentacene dimer.[56,97,98] Thus, dissociation of $^1(T_1T_1)_{Pnc2}$ into free triplets is unlikely, which is consistent with minimal observed yields for (T_1+T_1) of roughly 1% (Figures S35 and S37; Tables 1 and S5). Increasing solvent polarity does not affect the yield of (T_1+T_1) for DiPnc. The only potential influence of solvent polarity is a slightly faster formation and deactivation of $^1(T_1T_1)_{Pnc2}$ in a more polar environment. The corresponding lifetimes obtained by fitting the raw data (Figures 3a, 5a, S19, S21, S24, and S26) according to the

Table 1: Calculated excitation-wavelength (λ_{exc}) dependent free triplet (T_1+T_1) quantum yields (TQYs) of DiPnc and HexPnc.[a]

		DiPnc	HexPnc							
λ_{exc} [nm]		532/660	532		610		633		660	
			Pnc_2	Pnc_4	Pnc_2	Pnc_4	Pnc_2	Pnc_4	Pnc_2	Pnc_4
toluene	ratio	–	0.42	0.58	0.43	0.57	0.43	0.57	0.52	0.48
	(T_1+T_1)	≈1%	14%		14%		14%		12%	
benzonitrile	ratio	–	0.42	0.58	0.45	0.55	0.45	0.5	0.53	0.47
	(T_1+T_1)	≈1%	14%		14%		14%		12%	

[a] An error margin of ±20% is implicit in the determination of the (T_1+T_1) yields for HexPnc considering the complexity of the model, that is, a parallel deactivation mechanism with several spectroscopically indistinguishable species present simultaneously. This makes an exact differentiation between the Pnc_2 and Pnc_4 deactivation pathway challenging. In addition, the lifetime of $^M(T_1\cdots T_1)_{Pnc4}$ is both too long to be fully deconvoluted using fsTA spectroscopy and too short to be fully deconvoluted using nsTA spectroscopy, further contributing to the uncertainty in the calculated TQYs. Excitation ratios obtained from nsTA spectroscopy experiments were used for the calculations.

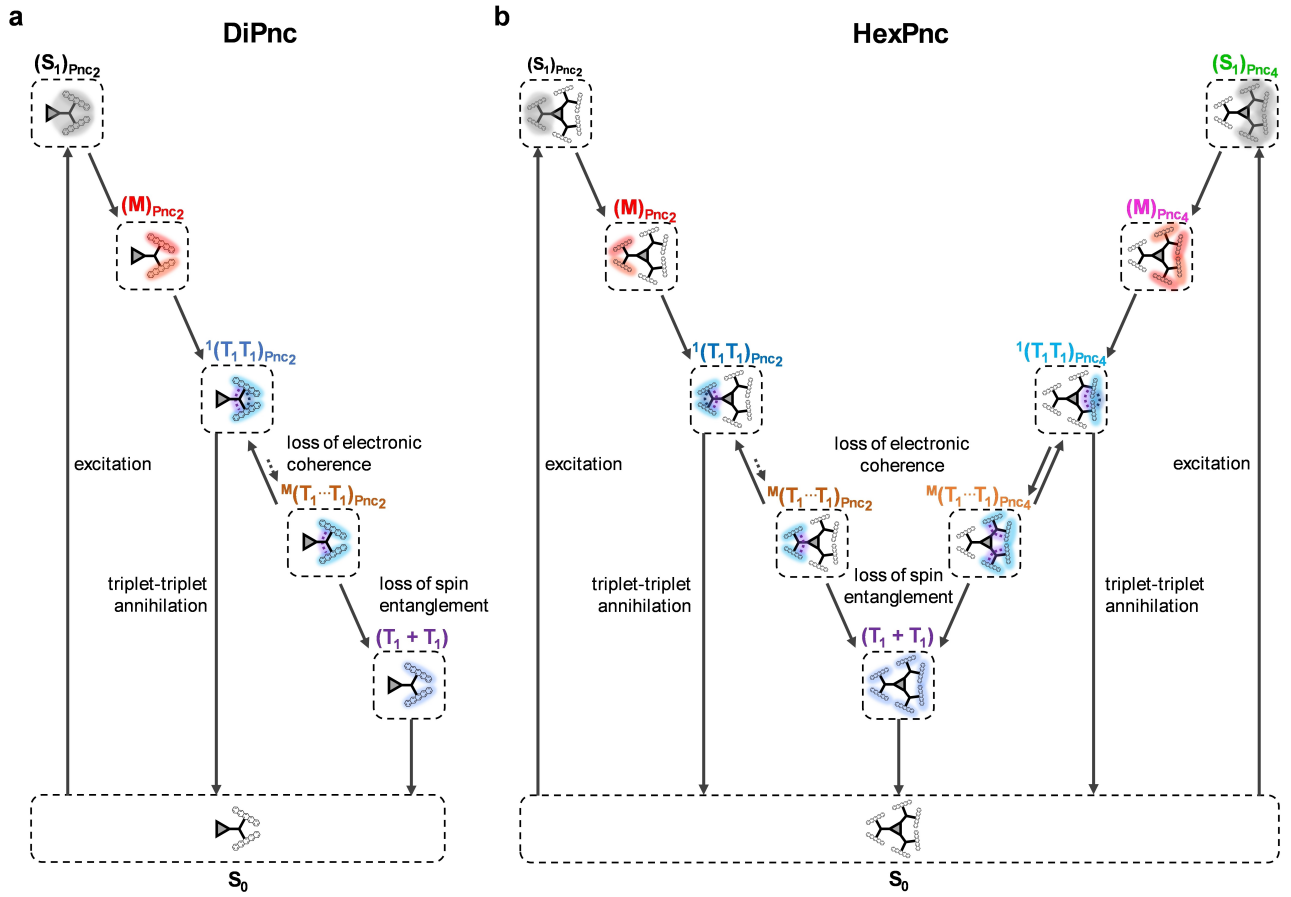

Figure 7. Proposed excited-state dynamics of (a) DiPnc and (b) HexPnc following photoexcitation (only direct excitation of pentacene is included, as *i*-FRET is too fast for deconvolution).[78] Both DiPnc and HexPnc undergo intramolecular singlet fission (*i*-SF), that is, the conversion of the first singlet excited state of pentacene (S_1) into the multiexciton state $^1(T_1T_1)$ via the mixed intermediate state (M). $^1(T_1T_1)$ may undergo intramolecular triplet-triplet annihilation or subsequently lose electronic coherence (indicated by the blue dotted line) first to produce a weakly coupled triplet pair state $^M(T_1\cdots T_1)$ before losing spin entanglement (indicated by the purple dotted line) to yield two free triplet excited states (T_1+T_1). *i*-SF and deactivation occur via a single channel for DiPnc, while two parallel deactivation channels are proposed for HexPnc, Pnc_2 and Pnc_4. The excitation ratio between Pnc_2 and Pnc_4 is modulated by the wavelength of the pump pulse and directly affects the overall rate of *i*-SF, as well as the yield of free triplet excited states. For simplicity, SubPc is depicted as a triangle. The localization of the respective states is indicated by the shading of the chromophores involved. The color scheme of the state labels corresponds to that in the following species-associated spectra.

mechanism shown in Figures 7, S29, and S34 are listed in Tables S3 and S4, and the obtained parameters are in excellent agreement with prior studies on structurally similar SubPc-Pnc_2 conjugates.[29,78,92,93]

For HexPnc, contributions from the Pnc_2 channel are modeled in the same way as in DiPnc. Similar to that of DiPnc, the correlated triplet pair $^1(T_1T_1)_{Pnc2}$ is subject to efficient TTA. A loss of electronic coherence, on the one hand, and subsequent spin dephasing, on the other hand, is unfavorable for Pnc_2, and excitation into Pnc_2 thus results in only a marginal contribution to the overall yields of (T_1+T_1) in comparison to DiPnc. In contrast, the Pnc_4 channel leads to substantially higher yields of $^M(T_1\cdots T_1)_{Pnc4}$ and (T_1+T_1). In addition to torsional and rotational motions, the possibility of spatial separation, i.e., the hopping of triplets between chromophores within the intramolecular cluster, fosters the loss of electronic couplings in $^1(T_1T_1)_{Pnc4}$. Overall, yields of (T_1+T_1) of HexPnc are considerably higher compared to those of DiPnc, reaching values of up to 14 % in both toluene and benzonitrile (Tables 1 and S5).

Despite the complexity of our kinetic model, which is warranted by the number of spectroscopically indistinguishable triplet excited state species, the good agreement between experimental data and obtained fits is striking. At 660 nm, only minor differences in the oscillator strength between Pnc_2 and Pnc_4 exist. This is reflected in a 60:40 (Pnc_2:Pnc_4) and 52:48 (Pnc_2:Pnc_4) excitation ratio for the fsTA and nsTA data, respectively, in toluene (Figure 8). Upon shortening of the excitation wavelength, for example at 633 nm, the excitation ratio shifts, now favoring excitation into the Pnc_4 subunit. Thus, an excitation ratio of 45:55 (Pnc_2:Pnc_4) and 43:57 (Pnc_2:Pnc_4) is required to fit the fsTA and nsTA data, respectively (Figures 8, S33c and S38c). Shifts in the excitation ratio are in line with our expectations, in light of the changes in the oscillator strengths found for pentacene derivatives when going from solution to the solid state (Figure 2a). For excitation at 610 nm, ratios

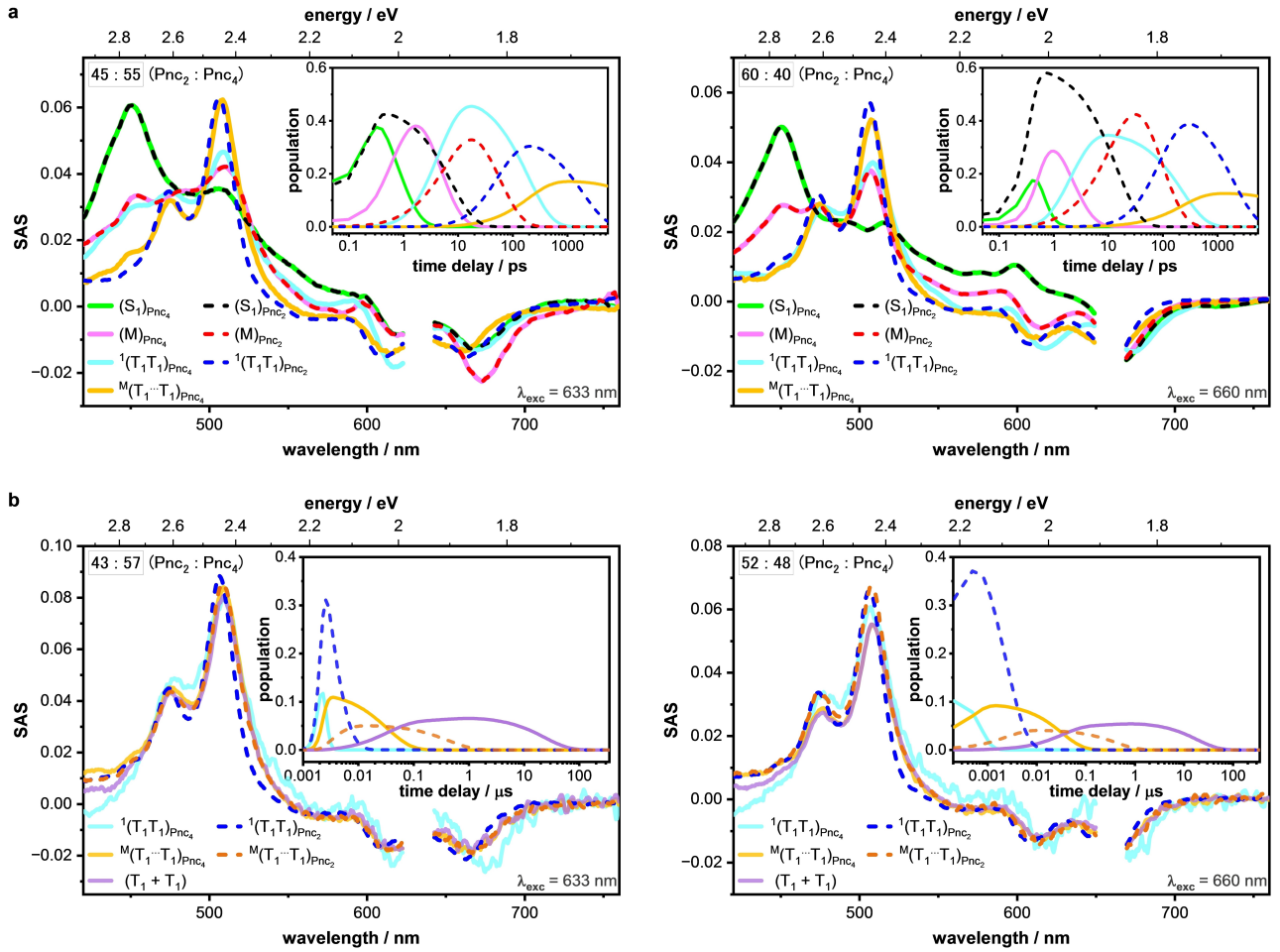

Figure 8. Species-associated spectra (SAS) of the femtosecond (a) and nanosecond (b) transient absorption data of HexPnc in toluene at room temperature (see Figures S29 (top) and S34 (bottom) for underlying deactivation mechanism). Insets depict the relative population of the respective states. Spectra following photoexcitation at 633 nm (left) and 660 nm (right) are shown to demonstrate the relationship between pump energy and branching ratio between the Pnc_4 and the Pnc_2 subunits, respectively (top left corner in each plot). Shorter excitation wavelengths result in an excitation ratio which favors excitation of the Pnc_4 subunit.

remain virtually identical to excitation at 633 nm (Figures S31b, S33b, S36b, and S38b). With photoexcitation at 532 nm, *i*-FRET is operative. The shortest SubPc-Pnc distances and highest dipolar couplings are found for pentacenes 2 and 3 (Figures S42–S49; Table S6). Since the magnitude of the dipolar couplings is proportional to the energy transfer rate (see SI, Section 8), we assume that *i*-FRET to Pnc_4 dominates over *i*-FRET to Pnc_2 which impacts the excitation ratio, in addition to stronger absorptions for Pnc_4 present at 532 nm due to the greater oscillator strength. This premise is further corroborated by the fact that $(S_1)_{Pnc4}$ carries some SubPc GSB, while $(S_1)_{Pnc2}$ does not (Figures S31a and S33a). All excitation ratios as a function of the excitation wavelength are listed in the Supporting Information (Tables S3 and S4). Deconvolution of $^1(T_1T_1)_{Pnc4}$ shows GSBs that are reminiscent of the ground-state bleaching of a drop-cast film of pentacene (Figures 8, S31, S33, S36, and S38). Relative to $^1(T_1T_1)_{Pnc2}$, the GSB is redshifted in $^1(T_1T_1)_{Pnc4}$ and the vibrational fine structure is altered. In general, the rates of *i*-SF within the Pnc_4 channel are substantially faster than for the Pnc_2 channel. The formation of $^1(T_1T_1)_{Pnc4}$ occurs within a few picoseconds, opposed to the evolution times of several tens of picoseconds within Pnc_2 (Figures S30–S33). Comparing the $^1(T_1T_1)$ formation rates in Pnc_4 with that of another hexameric pentacene system reported by the Kim group, in which only moderate through-space interactions are present, contrasts a few picoseconds with tens of picoseconds.[25,74] The triplet evolution dynamics of HexPnc are in better agreement with the picosecond $^1(T_1T_1)$ formation rates seen in other pentacene dendrimers,[75,76,102] which exhibit stronger through-space interactions derived from more tightly packed π-stacked conformations, and approach evolution times on the order of a few hundreds of femtoseconds, which is the same timeframe determined for pentacene films by fsTA experiments.[49,67,72,99,103–106] This is consistent with the calculated $^1(T_1T_1)$ yields, which are higher for the Pnc_4 subunit than for the Pnc_2 subunit (Table S5). The subsequent loss of electronic and vibronic coherence in the Pnc_4 deactivation channel, as well as spin dephasing, also take place on a time

scale that is an order of magnitude faster than in Pnc_2. This showcases the important role of entropically-driven triplet diffusion in the decorrelation of strongly coupled $^1(T_1T_1)$ states. It is noteworthy that lifetimes and $^1(T_1T_1)$ yields of the Pnc_2 subunit of HexPnc and those of DiPnc show remarkably good agreement (Figure S50; Tables S3–S5) and provide further corroboration for the postulated intramolecular cluster of pentacene units in HexPnc. In addition, striking similarities are noted between the triplet deactivation dynamics of HexPnc and the extended dendrimeric pentacene systems investigated by He et al.,[75] in which strongly and weakly coupled SF sites coexist. The dendrimer features faster $^1(T_1T_1)$ formation for the more strongly coupled interacting regions, in accordance with our observations for HexPnc comprising both the Pnc_2 and Pnc_4 channel. However, the fate of $^1(T_1T_1)$ in regions of strong electronic coupling is dominated by efficient TTA to afford the electronic ground state. As matter of fact, formation of free triplets stems from regions of weaker couplings. This is in stark contrast to our observations, where the more strongly coupled channel (Pnc_4) contributes significantly to the ultimate free triplet population.[75]

Conclusion

Our work on HexPnc shows that tethering multiple pentacene dimers to a central SubPc moiety is an elegant way to design a molecule that mimics a solid-state system. HexPnc exhibits strong interpentacene couplings that drive rapid intramolecular singlet fission (*i*-SF) and, nevertheless, achieves considerably increased yields of (T_1+T_1) in comparison to DiPnc by allowing for intramolecular triplet diffusion. Intramolecular cluster formation within HexPnc results in an unsymmetrical geometry that features a solid-state like agglomerate encompassing two pentacene units in a twisted slipped stack arrangement. This cluster plays a key role in achieving both rapid *i*-SF and high yields of triplet excited states, effectively achieving two desirable goals that are typically contradictory in covalent systems. This work highlights the significance of careful molecular engineering and provides design guidelines for concomitantly maximizing $^1(T_1T_1)$ formation as well as subsequent dissociation rates to (T_1+T_1). The arrangement of SF chromophores in larger arrays that enable spatial separation of the correlated triplet pair, while maintaining strong interchromophore couplings (coupling hot spots between one pair), is clearly beneficial for the optimization of these opposing processes.

Associated Content

Supporting Information is available for this paper at https://doi.org/10.1002/anie.202315064.

Author Contributions

R.R.T., D.M.G., M.B.N., and T.T. designed the project. H.G. designed the conjugates. H.G. and L.C. synthesized and characterized the compounds. P.M.G., D.T., and I.P. performed the steady-state and time-resolved photophysical experiments. M.K. and T.C. performed the quantum chemical calculations. M.M. performed the variable-temperature and diffusion NMR experiments. P.M.G., D.T., H.G, R.R.T., and D.M.G. wrote the paper. All authors discussed the results and edited the manuscript.

Acknowledgements

R.R.T. acknowledges funding from the Natural Sciences and Engineering Research Council of Canada (NSERC, grant no. RGPIN-2017-05052) and the Canada Foundation for Innovation (CFI). D.M.G. acknowledges financial support from the Deutsche Forschungsgemeinschaft (DFG) as part of SFB 953 "Synthetic Carbon Allotropes" and GU 517/32-1. T.T. acknowledges financial support from the Spanish MCIN/AEI/10.13039/501100011033 (PID2020-116490GB–I00, TED2021-131255B–C43), the Comunidad de Madrid and the Spanish State through the Recovery, Transformation and Resilience Plan ["Materiales Disruptivos Bidimensionales (2D)" (MAD2D-CM) (UAM1)-MRR Materiales Avanzados], and the European Union through the Next Generation EU funds. IMDEA Nanociencia acknowledges support from the "Severo Ochoa" Programme for Centres of Excellence in R&D (MINECO, Grant SEV2016-0686). T. T. also acknowledges the Alexander von Humboldt Foundation (Germany) for the A. v. Humboldt—J. C. Mutis Research Award 2023 (Ref [3].3-1231125—ESP-GSA). H.G. thanks the Danish Ministry of Higher Education and Science for an EliteForsk travel scholarship (6161-00051B). Open Access funding enabled and organized by Projekt DEAL.

Conflict of Interest

The authors declare no conflict of interest.

Data Availability Statement

The data that support the findings of this study are available from the corresponding author upon reasonable request.

Keywords: Oligoacene · Photoenergy Conversion · Singlet Fission · Triplet Dissociation · Ultrafast Spectroscopy

[1] W. Shockley, H. J. Queisser, *J. Appl. Phys.* **1961**, *32*, 510–519.
[2] L. C. Hirst, N. J. Ekins-Daukes, *Prog. Photovoltaics Res. Appl.* **2011**, *19*, 286–293.
[3] R. J. Hudson, A. N. Stuart, D. M. Huang, T. W. Kee, *J. Phys. Chem. C* **2022**, *126*, 5369–5377.

[4] C. A. Nelson, N. R. Monahan, X. Y. Zhu, *Energy Environ. Sci.* **2013**, *6*, 3508–3519.
[5] B. Ehrler, E. Alarcón-Lladó, S. W. Tabernig, T. Veeken, E. C. Garnett, A. Polman, *ACS Energy Lett.* **2020**, *5*, 3029–3033.
[6] M. B. Smith, J. Michl, *Chem. Rev.* **2010**, *110*, 6891–6936.
[7] M. B. Smith, J. Michl, *Annu. Rev. Phys. Chem.* **2013**, *64*, 361–386.
[8] X. Zhu, *Acc. Chem. Res.* **2013**, *46*, 1239–1241.
[9] R. Casillas, I. Papadopoulos, T. Ullrich, D. Thiel, A. Kunzmann, D. M. Guldi, *Energy Environ. Sci.* **2020**, *13*, 2741–2804.
[10] T. Ullrich, D. Munz, D. M. Guldi, *Chem. Soc. Rev.* **2021**, *50*, 3485–3518.
[11] D. Casanova, *Chem. Rev.* **2018**, *118*, 7164–7207.
[12] A. Rao, R. H. Friend, *Nat. Rev. Mater.* **2017**, *2*, 17063.
[13] K. E. Smyser, J. D. Eaves, *Sci. Rep.* **2020**, *10*, 18480.
[14] K. Miyata, F. S. Conrad-Burton, F. L. Geyer, X. Y. Zhu, *Chem. Rev.* **2019**, *119*, 4261–4292.
[15] M. J. Y. Tayebjee, A. A. Gray-Weale, T. W. Schmidt, *J. Phys. Chem. Lett.* **2012**, *3*, 2749–2754.
[16] M. J. Y. Tayebjee, D. R. McCamey, T. W. Schmidt, *J. Phys. Chem. Lett.* **2015**, *6*, 2367–2378.
[17] A. Kunzmann, M. Gruber, R. Casillas, J. Zirzlmeier, M. Stanzel, W. Peukert, R. R. Tykwinski, D. M. Guldi, *Angew. Chem. Int. Ed.* **2018**, *57*, 10742–10747.
[18] M. C. Hanna, A. J. Nozik, *J. Appl. Phys.* **2006**, *100*, 074510.
[19] W.-L. Chan, M. Ligges, A. Jailaubekov, L. Kaake, L. Miaja-Avila, X.-Y. Zhu, *Science* **2011**, *334*, 1541–1545.
[20] R. D. Pensack, E. E. Ostroumov, A. J. Tilley, S. Mazza, C. Grieco, K. J. Thorley, J. B. Asbury, D. S. Seferos, J. E. Anthony, G. D. Scholes, *J. Phys. Chem. Lett.* **2016**, *7*, 2370–2375.
[21] I. Breen, R. Tempelaar, L. A. Bizimana, B. Kloss, D. R. Reichman, D. B. Turner, *J. Am. Chem. Soc.* **2017**, *139*, 11745–11751.
[22] W. Kim, A. J. Musser, *Adv. Phys. X* **2021**, *6*, 1918022.
[23] R. M. Young, M. R. Wasielewski, *Acc. Chem. Res.* **2020**, *53*, 1957–1968.
[24] R. D. Pensack, G. E. Purdum, S. M. Mazza, C. Grieco, J. B. Asbury, J. E. Anthony, Y.-L. Loo, G. D. Scholes, *J. Phys. Chem. C* **2022**, *126*, 9784–9793.
[25] J. Kim, H. T. Teo, Y. Hong, J. Oh, H. Kim, C. Chi, D. Kim, *Angew. Chem. Int. Ed.* **2020**, *59*, 20956–20964.
[26] M. K. Gish, N. A. Pace, G. Rumbles, J. C. Johnson, *J. Phys. Chem. C* **2019**, *123*, 3923–3934.
[27] B. S. Basel, I. Papadopoulos, D. Thiel, R. Casillas, J. Zirzlmeier, T. Clark, D. M. Guldi, R. R. Tykwinski, *Trends Chem.* **2019**, *1*, 11–21.
[28] B. S. Basel, J. Zirzlmeier, C. Hetzer, B. T. Phelan, M. D. Krzyaniak, S. R. Reddy, P. B. Coto, N. E. Horwitz, R. M. Young, F. J. White, F. Hampel, T. Clark, M. Thoss, R. R. Tykwinski, M. R. Wasielewski, D. M. Guldi, *Nat. Commun.* **2017**, *8*, 15171.
[29] J. Zirzlmeier, D. Lehnherr, P. B. Coto, E. T. Chernick, R. Casillas, B. S. Basel, M. Thoss, R. R. Tykwinski, D. M. Guldi, *Proc. Natl. Acad. Sci. USA* **2015**, *112*, 5325–5330.
[30] B. S. Basel, J. Zirzlmeier, C. Hetzer, S. R. Reddy, B. T. Phelan, M. D. Krzyaniak, M. K. Volland, P. B. Coto, R. M. Young, T. Clark, M. Thoss, R. R. Tykwinski, M. R. Wasielewski, D. M. Guldi, *Chem* **2018**, *4*, 1092–1111.
[31] N. V. Korovina, S. Das, Z. Nett, X. Feng, J. Joy, R. Haiges, A. I. Krylov, S. E. Bradforth, M. E. Thompson, *J. Am. Chem. Soc.* **2016**, *138*, 617–627.
[32] N. Alagna, J. L. Pérez Lustres, N. Wollscheid, Q. Luo, J. Han, A. Dreuw, F. L. Geyer, V. Brosius, U. H. F. Bunz, T. Buckup, M. Motzkus, *J. Phys. Chem. B* **2019**, *123*, 10780–10793.
[33] S. N. Sanders, E. Kumarasamy, A. B. Pun, M. T. Trinh, B. Choi, J. Xia, E. J. Taffet, J. Z. Low, J. R. Miller, X. Roy, X. Y. Zhu, M. L. Steigerwald, M. Y. Sfeir, L. M. Campos, *J. Am. Chem. Soc.* **2015**, *137*, 8965–8972.
[34] D. N. Congreve, J. Lee, N. J. Thompson, E. Hontz, S. R. Yost, P. D. Reusswig, M. E. Bahlke, S. Reineke, T. Van Voorhis, M. A. Baldo, *Science* **2013**, *340*, 334–337.
[35] J. J. Burdett, C. J. Bardeen, *J. Am. Chem. Soc.* **2012**, *134*, 8597–8607.
[36] E. G. Fuemmeler, S. N. Sanders, A. B. Pun, E. Kumarasamy, T. Zeng, K. Miyata, M. L. Steigerwald, X. Y. Zhu, M. Y. Sfeir, L. M. Campos, N. Ananth, *ACS Cent. Sci.* **2016**, *2*, 316–324.
[37] B. S. Basel, R. M. Young, M. D. Krzyaniak, I. Papadopoulos, C. Hetzer, Y. Gao, N. T. La Porte, B. T. Phelan, T. Clark, R. R. Tykwinski, M. R. Wasielewski, D. M. Guldi, *Chem. Sci.* **2019**, *10*, 11130–11140.
[38] C. Hetzer, D. M. Guldi, R. R. Tykwinski, *Chem. Eur. J.* **2018**, *24*, 8245–8257.
[39] T. C. Berkelbach, M. S. Hybertsen, D. R. Reichman, *J. Chem. Phys.* **2013**, *138*, 114103.
[40] N. Monahan, X. Y. Zhu, *Annu. Rev. Phys. Chem.* **2015**, *66*, 601–618.
[41] E. A. Margulies, C. E. Miller, Y. Wu, L. Ma, G. C. Schatz, R. M. Young, M. R. Wasielewski, *Nat. Chem.* **2016**, *8*, 1120–1125.
[42] S. Ito, T. Nagami, M. Nakano, *J. Photochem. Photobiol. C* **2018**, *34*, 85–120.
[43] M. Chen, Y. J. Bae, C. M. Mauck, A. Mandal, R. M. Young, M. R. Wasielewski, *J. Am. Chem. Soc.* **2018**, *140*, 9184–9192.
[44] M. Chen, M. D. Krzyaniak, J. N. Nelson, Y. J. Bae, S. M. Harvey, R. D. Schaller, R. M. Young, M. R. Wasielewski, *Proc. Natl. Acad. Sci. USA* **2019**, *116*, 8178–8183.
[45] A. Mandal, M. Chen, E. D. Foszcz, J. D. Schultz, N. M. Kearns, R. M. Young, M. T. Zanni, M. R. Wasielewski, *J. Am. Chem. Soc.* **2018**, *140*, 17907–17914.
[46] Y. Hong, J. Kim, W. Kim, C. Kaufmann, H. Kim, F. Würthner, D. Kim, *J. Am. Chem. Soc.* **2020**, *142*, 7845–7857.
[47] A. V. Akimov, O. V. Prezhdo, *J. Chem. Theory Comput.* **2014**, *10*, 789–804.
[48] H. Sakai, R. Inaya, H. Nagashima, S. Nakamura, Y. Kobori, N. V. Tkachenko, T. Hasobe, *J. Phys. Chem. Lett.* **2018**, *9*, 3354–3360.
[49] H. Huang, G. He, K. Xu, Q. Wu, D. Wu, M. Y. Sfeir, J. Xia, *Chem* **2019**, *5*, 2405–2417.
[50] E. Kumarasamy, S. N. Sanders, M. J. Y. Tayebjee, A. Asadpoordarvish, T. J. H. Hele, E. G. Fuemmeler, A. B. Pun, L. M. Yablon, J. Z. Low, D. W. Paley, J. C. Dean, B. Choi, G. D. Scholes, M. L. Steigerwald, N. Ananth, D. R. McCamey, M. Y. Sfeir, L. M. Campos, *J. Am. Chem. Soc.* **2017**, *139*, 12488–12494.
[51] N. V. Korovina, C. H. Chang, J. C. Johnson, *Nat. Chem.* **2020**, *12*, 391–398.
[52] Z. Wang, H. Liu, X. Xie, C. Zhang, R. Wang, L. Chen, Y. Xu, H. Ma, W. Fang, Y. Yao, H. Sang, X. Wang, X. Li, M. Xiao, *Nat. Chem.* **2021**, *13*, 559–567.
[53] A. M. Müller, Y. S. Avlasevich, W. W. Schoeller, K. Müllen, C. J. Bardeen, *J. Am. Chem. Soc.* **2007**, *129*, 14240–14250.
[54] X. Wang, R. Wang, L. Shen, Z. Tang, C. Wen, B. Dong, H. Liu, C. Zhang, X. Li, *Phys. Chem. Chem. Phys.* **2018**, *20*, 6330–6336.
[55] R. D. Pensack, A. J. Tilley, C. Grieco, G. E. Purdum, E. E. Ostroumov, D. B. Granger, D. G. Oblinsky, J. C. Dean, G. S. Doucette, J. B. Asbury, Y.-L. Loo, D. S. Seferos, J. E. Anthony, G. D. Scholes, *Chem. Sci.* **2018**, *9*, 6240–6259.
[56] R. Xu, C. Zhang, M. Xiao, *Trends Chem.* **2022**, *4*, 528–539.

[57] M. J. Y. Tayebjee, S. N. Sanders, E. Kumarasamy, L. M. Campos, M. Y. Sfeir, D. R. McCamey, *Nat. Phys.* **2017**, *13*, 182–188.
[58] E. J. Taffet, D. Beljonne, G. D. Scholes, *J. Am. Chem. Soc.* **2020**, *142*, 20040–20047.
[59] H. Nagashima, S. Kawaoka, S. Akimoto, T. Tachikawa, Y. Matsui, H. Ikeda, Y. Kobori, *J. Phys. Chem. Lett.* **2018**, *9*, 5855–5861.
[60] C. Grieco, G. S. Doucette, J. M. Munro, E. R. Kennehan, Y. Lee, A. Rimshaw, M. M. Payne, N. Wonderling, J. E. Anthony, I. Dabo, E. D. Gomez, J. B. Asbury, *Adv. Funct. Mater.* **2017**, *27*, 1703929.
[61] M. Wakasa, M. Kaise, T. Yago, R. Katoh, Y. Wakikawa, T. Ikoma, *J. Phys. Chem. C* **2015**, *119*, 25840–25844.
[62] T. Zhu, L. Huang, *J. Phys. Chem. Lett.* **2018**, *9*, 6502–6510.
[63] N. V. Korovina, N. F. Pompetti, J. C. Johnson, *J. Chem. Phys.* **2020**, *152*, 040904.
[64] C. Hetzer, B. S. Basel, S. M. Kopp, F. Hampel, F. J. White, T. Clark, D. M. Guldi, R. R. Tykwinski, *Angew. Chem. Int. Ed.* **2019**, *58*, 15263–15267.
[65] S. Nakamura, H. Sakai, M. Fuki, R. Ooie, F. Ishiwari, A. Saeki, N. V. Tkachenko, Y. Kobori, T. Hasobe, *Angew. Chem. Int. Ed.* **2023**, *62*, e202217704.
[66] A. J. Musser, J. Clark, *Annu. Rev. Phys. Chem.* **2019**, *70*, 323–351.
[67] A. N. Stuart, P. C. Tapping, E. Schrefl, D. M. Huang, T. W. Kee, *J. Phys. Chem. C* **2019**, *123*, 5813–5825.
[68] M. Tuan Trinh, A. Pinkard, A. B. Pun, S. N. Sanders, E. Kumarasamy, M. Y. Sfeir, L. M. Campos, X. Roy, X. Y. Zhu, *Sci. Adv.* **2017**, *3*, e1700241.
[69] S. N. Sanders, E. Kumarasamy, A. B. Pun, K. Appavoo, M. L. Steigerwald, L. M. Campos, M. Y. Sfeir, *J. Am. Chem. Soc.* **2016**, *138*, 7289–7297.
[70] C. K. Yong, A. J. Musser, S. L. Bayliss, S. Lukman, H. Tamura, O. Bubnova, R. K. Hallani, A. Meneau, R. Resel, M. Maruyama, S. Hotta, L. M. Herz, D. Beljonne, J. E. Anthony, J. Clark, H. Sirringhaus, *Nat. Commun.* **2017**, *8*, 15953.
[71] T. Wang, H. Liu, X. Wang, L. Tang, J. Zhou, X. Song, L. Lv, W. Chen, Y. Chen, X. Li, *J. Mater. Chem. A* **2023**, *11*, 8515–8539.
[72] R. D. Pensack, A. J. Tilley, S. R. Parkin, T. S. Lee, M. M. Payne, D. Gao, A. A. Jahnke, D. G. Oblinsky, P. F. Li, J. E. Anthony, D. S. Seferos, G. D. Scholes, *J. Am. Chem. Soc.* **2015**, *137*, 6790–6803.
[73] G. He, L. M. Yablon, K. R. Parenti, K. J. Fallon, L. M. Campos, M. Y. Sfeir, *J. Am. Chem. Soc.* **2022**, *144*, 3269–3278.
[74] J. Kim, H. T. Teo, Y. Hong, Y. C. Liau, D. Yim, Y. Han, J. Oh, H. Kim, C. Chi, D. Kim, *J. Am. Chem. Soc.* **2023**, *145*, 19812–19823.
[75] G. He, E. M. Churchill, K. R. Parenti, J. Zhang, P. Narayanan, F. Namata, M. Malkoch, D. N. Congreve, A. Cacciuto, M. Y. Sfeir, L. M. Campos, *Nat. Commun.* **2023**, *14*, 6080.
[76] S. R. E. Orsborne, J. Gorman, L. R. Weiss, A. Sridhar, N. A. Panjwani, G. Divitini, P. Budden, D. Palecek, S. T. J. Ryan, A. Rao, R. Collepardo-Guevara, A. H. El-Sagheer, T. Brown, J. Behrends, R. H. Friend, F. Auras, *J. Am. Chem. Soc.* **2023**, *145*, 5431–5438.
[77] G. Lavarda, J. Labella, M. V. Martínez-Díaz, M. S. Rodríguez-Morgade, A. Osuka, T. Torres, *Chem. Soc. Rev.* **2022**, *51*, 9482–9619.
[78] H. Gotfredsen, D. Thiel, P. M. Greißel, L. Chen, M. Krug, I. Papadopoulos, M. J. Ferguson, M. B. Nielsen, T. Torres, T. Clark, D. M. Guldi, R. R. Tykwinski, *J. Am. Chem. Soc.* **2023**, *145*, 9548–9563.
[79] N. A. Pace, N. V. Korovina, T. T. Clikeman, S. Holliday, D. B. Granger, G. M. Carroll, S. U. Nanayakkara, J. E. Anthony, I. McCulloch, S. H. Strauss, O. V. Boltalina, J. C. Johnson, G. Rumbles, O. G. Reid, *Nat. Chem.* **2020**, *12*, 63–70.
[80] C. G. Claessens, M. J. Vicente-Arana, T. Torres, *Chem. Commun.* **2008**, 6378.
[81] D. González-Rodríguez, T. Torres, D. M. Guldi, J. Rivera, M. Á. Herranz, L. Echegoyen, *J. Am. Chem. Soc.* **2004**, *126*, 6301–6313.
[82] C. G. Claessens, T. Torres, *Tetrahedron Lett.* **2000**, *41*, 6361–6365.
[83] F. Würthner, C. R. Saha-Möller, B. Fimmel, S. Ogi, P. Leowanawat, D. Schmidt, *Chem. Rev.* **2016**, *116*, 962–1052.
[84] N. J. Hestand, F. C. Spano, *J. Chem. Phys.* **2015**, *143*, 244707.
[85] B. S. Basel, C. Hetzer, J. Zirzlmeier, D. Thiel, R. Guldi, F. Hampel, A. Kahnt, T. Clark, D. M. Guldi, R. R. Tykwinski, *Chem. Sci.* **2019**, *10*, 3854–3863.
[86] The prospect of intermolecular aggregations was discounted based on DOSY NMR experiments.
[87] In order to reduce computational costs, the solubilizing groups iBu$_3$ and tBu of HexPnc and DiPnc have been replaced by methyl groups and hydrogen atoms, respectively.
[88] In solution, interconversion between these lowest-energy conformers cannot be excluded at room temperature. Such interconversion, however, would occur on a microsecond timescale, which is slow compared to the excited-state dynamics probed by femtosecond- and nanosecond transient absorption experiments.
[89] A. B. Pun, S. N. Sanders, E. Kumarasamy, M. Y. Sfeir, D. N. Congreve, L. M. Campos, *Adv. Mater.* **2017**, *29*, 1701416.
[90] The error margin for calculating non-covalent interactions in complex systems is in the range of 10 to 20%. S. Ehrlich, J. Moellmann, S. Grimme, *Acc. Chem. Res.* **2013**, *46*, 916–926.
[91] B3LYP+GD3BJ tends to overestimate dispersive interactions. N. M. Kreienborg, C. Merten, *Chem. Eur. J.* **2018**, *24*, 17948–17954.
[92] G. Lavarda, J. Zirzlmeier, M. Gruber, P. R. Rami, R. R. Tykwinski, T. Torres, D. M. Guldi, *Angew. Chem. Int. Ed.* **2018**, *57*, 16291–16295.
[93] D. P. Medina, I. Papadopoulos, G. Lavarda, H. Gotfredsen, P. R. Rami, R. R. Tykwinski, M. S. Rodríguez-Morgade, D. M. Guldi, T. Torres, *Nanoscale* **2019**, *11*, 22286–22292.
[94] In contrast, DiPnc shows no evidence of an excitation wavelength dependency, which is in line with our expectations, considering that only one pentacene dimer is incorporated into the conjugate.
[95] A. Thampi, H. L. Stern, A. Cheminal, M. J. Y. Tayebjee, A. J. Petty, J. E. Anthony, A. Rao, *J. Am. Chem. Soc.* **2018**, *140*, 4613–4622.
[96] As we cannot selectively excite the Pnc$_4$ or Pnc$_2$ subunit of HexPnc, we can only make statements regarding the overall rate of i-SF, which is a weighted average of i-SF from Pnc$_4$ and Pnc$_2$. The respective contributions depend on the excitation wavelength.
[97] M. I. Collins, D. R. McCamey, M. J. Y. Tayebjee, *J. Chem. Phys.* **2019**, *151*, 164104.
[98] N. V. Korovina, J. Joy, X. Feng, C. Feltenberger, A. I. Krylov, S. E. Bradforth, M. E. Thompson, *J. Am. Chem. Soc.* **2018**, *140*, 10179–10190.
[99] T. S. Lee, Y. L. Lin, H. Kim, R. D. Pensack, B. P. Rand, G. D. Scholes, *J. Phys. Chem. Lett.* **2018**, *9*, 4087–4095.
[100] The same situation holds for DiPnc and explains the considerably lower population of free triplet excited states.
[101] Analyses of the triplet deactivation dynamics reveal that the triplet decay in HexPnc modeled with a tri-exponential decay function (that takes into account two intermediate triplet pair states) results in only poor fits.

[102] L. M. Yablon, S. N. Sanders, H. Li, K. R. Parenti, E. Kumarasamy, K. J. Fallon, M. J. A. Hore, A. Cacciuto, M. Y. Sfeir, L. M. Campos, *J. Am. Chem. Soc.* **2019**, *141*, 9564–9569.
[103] R. D. Pensack, C. Grieco, G. E. Purdum, S. M. Mazza, A. J. Tilley, E. E. Ostroumov, D. S. Seferos, Y.-L. Loo, J. B. Asbury, J. E. Anthony, G. D. Scholes, *Mater. Horiz.* **2017**, *4*, 915–923.
[104] C. Grieco, G. S. Doucette, R. D. Pensack, M. M. Payne, A. Rimshaw, G. D. Scholes, J. E. Anthony, J. B. Asbury, *J. Am. Chem. Soc.* **2016**, *138*, 16069–16080.
[105] S. R. Yost, J. Lee, M. W. B. Wilson, T. Wu, D. P. McMahon, R. R. Parkhurst, N. J. Thompson, D. N. Congreve, A. Rao, K. Johnson, M. Y. Sfeir, M. G. Bawendi, T. M. Swager, R. H. Friend, M. A. Baldo, T. Van Voorhis, *Nat. Chem.* **2014**, *6*, 492–497.
[106] A. J. Musser, M. Liebel, C. Schnedermann, T. Wende, T. B. Kehoe, A. Rao, P. Kukura, *Nat. Phys.* **2015**, *11*, 352–357.

Manuscript received: October 7, 2023
Accepted manuscript online: December 13, 2023
Version of record online: January 24, 2024

Research Articles

Photochemistry

P. M. Greißel, D. Thiel, H. Gotfredsen, L. Chen, M. Krug, I. Papadopoulos, M. Miskolzie, T. Torres, T. Clark, M. Brøndsted Nielsen, R. R. Tykwinski,* D. M. Guldi* e202315064

Intramolecular Triplet Diffusion Facilitates Triplet Dissociation in a Pentacene Hexamer

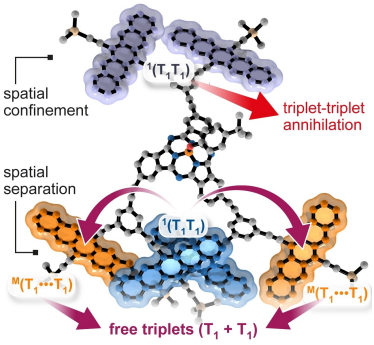

Efficient free triplet generation via singlet fission remains elusive in covalent systems. We have developed a hexameric pentacene system, in which three pentacene dimers are covalently linked to a central subphthalocyanine scaffold. This allows for an entropically driven triplet diffusion, resulting in higher yields of free triplets, and establishes crucial design aspects for achieving efficient triplet dissociation in strongly coupled systems.